A Novel Ray-Tracing Algorithm for Non-specular Diffuse Scattered Rays at Terahertz Frequencies

Fawad Sheikh*, Dien Lessy, and Thomas Kaiser
Institute of Digital Signal Processing
University of Duisburg-Essen, Campus Duisburg, NRW, Germany
E-mail: *fawad.sheikh@uni-due.de

***Abstract*—This paper presents a novel self-programmed three-dimensional (3D) ray-tracing algorithm (RTA) based on Beckmann-Kirchhoff (B-K) model for modeling diffuse scattering mechanism in non-specular directions at terahertz (THz) frequencies. The terahertz or submillimeter-wave frequencies pose unique challenges for channel modeling due to sparse and extreme frequency selective behaviour of the propagation mechanism. In particular, the most critical feature proved to provide important contributions in determining spatial and temporal dispersion in the submillimeter-wave band is the diffuse scattering mechanism, wherein an incident ray may split into a specular and several non-specular (diffused scattered) rays after bouncing off from rough materials. This makes the diffuse scattering or scattering from rough surfaces a necessary design consideration constituting a high proportion of all the propagation rays and hence, must be accounted for propagation modeling to accurately predict channel characteristics. Next, we integrate our MATLAB-based proposed algorithm to a commercial ray-tracing tool to derive a spatio-temporal model of scattered multipath propagation channels considering rough materials in a realistic office environment for both line-of-sight (LoS) and non-line-of-sight (NLoS) scenarios. So far none of the commercially available ray-tracing tools have implemented this scattering model yet.**

Keywords—THz communication, diffuse reflection, ray-tracing, rough surfaces, Kirchhoff scattering theory, Beckmann-Kirchhoff model, surface scattering.

I. INTRODUCTION

Submillimeter-wave or Terahertz (THz) band have the portion of the electromagnetic spectrum between 0.3 THz and 10 THz, considered to be the next last frontier for wireless communications. The THz band, sometimes referred to as the forbidden region due to technological limitations along with the enormous potential of THz communication technology particularly for short-range communication extends the research of channel propagation modeling. The existing models and tools in the lower frequency bands (i.e., 2.4 GHz, 5 GHz, Ultra-Wideband, 60 GHz) do not consider the roughness of material profoundly because materials smooth for GHz frequencies become rough now for terahertz frequencies. In consequence, it demands ray-tracing algorithms or simulation tools that can be employed for channel modeling at terahertz frequencies.

Nowadays, ray-tracing has becomes an attractive tool to simulate propagation channel, but most of the ray-tracing tools currently provide modeling up to GHz frequencies only. Hence, this cause for a high demand to develop ray-tracing algorithm which can also consider distinct terahertz propagation mechanisms such as atmospheric attenuation and diffuse scattering (non-specular reflections). Effective Roughness (ER) model can be utilized to model diffuse scattering as proposed in [1]. A 3D ray-tracing model including this ER model [2] shows a substantial improvement in prediction accuracy as compared to the conventional ray-tracing. However, this model does not consider correlation length or irregularity of surface fluctuation of the material and the direction of incidence [3]. By comparison, B-K model [4] is well-known for modeling not only specular reflection paths [5] but also diffuse scattered paths [6], where it takes into account the correlation length and incidence direction of the diffuse scattered paths.

In the present work, a novel self-programmed 3D ray-tracing algorithm (RTA) based on B-K model has been developed and validated against measurements in [7] at terahertz frequencies. Besides the basic propagation mechanism such as line-of-sight propagation, specular reflections, and diffraction, the developed RTA also employs the critical feature of THz propagation mechanisms such as specular reflection losses, diffuse scattering, depolarization, atmospheric attenuation and high reflection losses of indoor common building materials.

II. TERAHERTZ PROPAGATION MECHANISM

We briefly describe the individual propagation mechanisms of the ray-tracing with a view to provide an overall multipath scattering model of the indoor terahertz wireless channel. Note that we mention only the essential propagation mechanisms by neglecting the transmission, since indoor material thicknesses in the order of few centimeters have the transmission attenuations larger than several 10 dB and easily rise up to several 100 dB already in case of brick wall [8]. Thereupon, transmission will never contribute to the multipath propagation in indoor scenarios and can most often be disregarded at THz frequencies. The multipath scattering model for LoS propagation, reflected (specular), diffracted and diffuse scattered (non-specular) paths is given in (1).

$$E_{\mathrm{RX}} = E_{\mathrm{LoS}} + E_{\mathrm{Ref}} + E_{\mathrm{Diff}} + E_{\mathrm{Scatt}} \tag{1}$$

A. Line-of-Sight Propagation

Line-of-Sight propagation (or direct path) is the most simplest mode in which the propagation path between transmitter and receiver does not consider any interaction with absorbing or reflecting materials. It is also referred to as free space propagation. The line-of-sight electric field E_{LoS} received by

978-1-5386-1221-7/18/$31.00 ©2018 IEEE

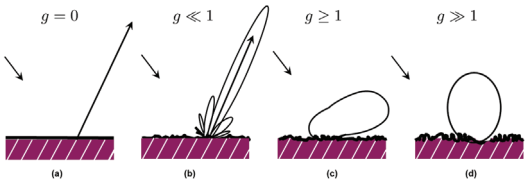

Fig. 1: Transition from specular reflection to diffuse scattering. The surfaces are: (a) smooth, (b) slightly rough, (c) moderately rough, and (d) very rough. Figure adapted from Fig. 5.1 in [4].

an (RX) antenna accounting the polarization vector as well as antenna gain G^{RX}, and relating to the emitted field E_{TX} radiated by the transmitter antenna (TX) with polarization and antenna gain G^{TX} is obtained as [9]

$$E_{\mathrm{LoS}} = \left[G^{\mathrm{RX}}_{\mathrm{LoS}}\right]^{*} \,.\, G^{\mathrm{TX}}_{\mathrm{LoS}} \,.\, L_{\mathrm{LoS}} \,.\, E_{\mathrm{TX}} \tag{2}$$

At THz frequencies, the line-of-sight propagation is not only affected by the free space path loss (FSPL), i.e. spreading of energy, the power is also lost along a transmission path due to the phenomena called molecular absorption or atmospheric attenuation. Therefore, the term L_{LoS} includes both of these losses.

B. Reflection

A reliable communication link can be guaranteed only if a THz communication system utilizes indirect paths (i.e., reflections) as a backup. At THz frequencies, in case of ideal smooth and homogeneous surfaces such as glass and wood, the characteristics of the reflection can be described by the well known Fresnel reflection coefficient. The reflection coefficient Γ depends not only on the angle of incidence and the electrical properties (permittivity, permeability, and conductivity) of the reflecting material, but also on the polarization of the incident wave. The authors in [10] have experimentally calculated the reflection coefficients from the frequency dependent index of refraction and absorption coefficient in the THz range. The Fresnel reflection coefficient expressions for parallel (Γ_{TM}) and perpendicular (Γ_{TE}) polarizations for smooth surfaces can be found in [4, p. 21].

To account for decrease in the reflected energy in specular direction due to the roughness of materials, Fresnel reflection coefficients must be multiplied by the Rayleigh roughness factor [4]. Notice that the scattering losses for the specular reflections is equal to the Rayleigh roughness factor (ρ_{spec}) as

$$\rho_{\mathrm{spec}} = e^{-\frac{g}{2}} = \exp\left(-\frac{8\pi^2 f^2 \sigma_h^2 \cos^2\Theta_i}{c^2}\right) \tag{3}$$

Here, g the roughness parameter of a material, f the frequency of incident wave, σ_h the standard deviation of surface roughness, Θ_i the angle of incidence and reflection relative to surface normal, and c the velocity of light. The parameter g is depicted with its reflection and scattering pattern in Fig. 1.

The modified reflection coefficients for parallel $\widetilde{\Gamma}_{\mathrm{TM}}$ and perpendicular $\widetilde{\Gamma}_{\mathrm{TE}}$ polarizations for rough surfaces are then

$$\widetilde{\Gamma}_{\mathrm{TE}} = \rho_{\mathrm{spec}}\, \Gamma_{\mathrm{TE}} \tag{4}$$

and

$$\widetilde{\Gamma}_{\mathrm{TM}} = \rho_{\mathrm{spec}}\, \Gamma_{\mathrm{TM}} \tag{5}$$

When the considered reflection point belongs to the dimension of the surface, the first order reflected field at the receiving point O can be expressed as [9]

$$E_{\mathrm{Ref}}(O) = \left[G^{\mathrm{RX}}_{\mathrm{Ref}}\right]^{*} \,.\, \mathbf{H} \,.\, G^{\mathrm{TX}}_{\mathrm{Ref}} \,.\, L_{\mathrm{Ref}} \,.\, E_{\mathrm{TX}} \tag{6}$$

where

$$\mathbf{H} = \mathbf{R}_{\mathrm{RX}} \times \begin{pmatrix} \widetilde{\Gamma}_{\mathrm{TE}} & \zeta_1 \\ \zeta_2 & \widetilde{\Gamma}_{\mathrm{TM}} \end{pmatrix} \times \mathbf{R}_{\mathrm{TX}} \tag{7}$$

Please note that the path length of reflections in L_{Ref} is the path length from TX to reflection point and the path length from reflection point to point O. The ζ_1 and ζ_2 are cross polarization coupling coefficients. For specular reflection paths, these coefficients are equal to zero [11]. Note that $\mathbf{R}_{\mathrm{RX}}$ and $\mathbf{R}_{\mathrm{TX}}$ are the geometrical depolarization vectors from receiver and transmitter, respectively [12].

C. Diffraction

Diffraction occurs when an obstacle with sharp irregularities (i.e., wedges, edges and circular cylinders) and large dimensions as compared to the propagated wavelength comes between transmitter and receiver. Even a moving person blocking the path of an electromagnetic wave can be considered as a diffracting object at terahertz frequencies [13]. Apart from persons, the diffracting objects in an indoor environment are metallic or wooden edges of file cabinets, bookshelves, cupboards, tables, workplace-privacy panels, open windows and doors. Due to diffraction phenomena, the propagated wave bends around the obstacle and continues propagating in the geometrical shadow region behind the obstacles. The well-known models with analytical description of the diffraction behaviour of many different objects are the uniform theory of diffraction (UTD) [14] and the knife edge diffraction (KED) [15]. The first approach not only holds valid for various objects with arbitrary dielectric parameters, but also accounts for polarization in contrast to the latter approach. However, the complexity of UTD is very high and it requires numerical solutions for path loss [8]. The first order diffracted field at the receiving point O can be expressed as [9]

$$E_{\mathrm{Diff}} = \left[G^{\mathrm{RX}}_{\mathrm{Diff}}\right]^{*} \,.\, G^{\mathrm{TX}}_{\mathrm{Diff}} \,.\, D \,.\, A \,.\, L_{\mathrm{Diff}} \,.\, E_{\mathrm{TX}} \tag{8}$$

Based on (12), E_{Diff} depends on D and A. The diffraction coefficient D is determined by diffraction angles at objects and the boundary conditions. Likewise, the geometry factor A considers the distance from TX and RX to the wedge.

D. Diffuse Scattering

Diffuse scattering is the most critical and important propagation phenomenon at terahertz frequencies. When an electromagnetic wave is incident on a rough surface, the phenomenon of diffuse scattering takes place splitting the wave into a specular and many scattered paths. When a wave is scattered, the resulting reflections occur in many directions, though certain privileged directions may receive more energy. The general scattering geometry is schematically shown in Fig. 2.

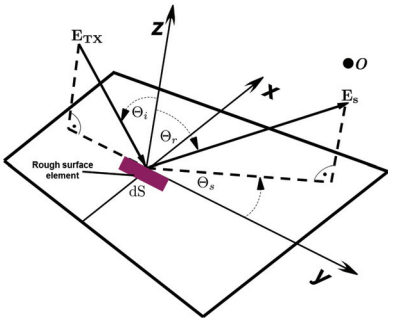

Fig. 2: The diffuse scattering from a rough surface element $\boldsymbol{dS}$.

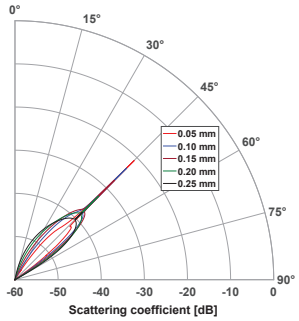

Fig. 3: Simulated scattering coefficient at 300 GHz of the plaster sample X_i, (d = 5 m).

Beckmann-Kirchhoff Scattering Model

In case of very rough surfaces, the reflection behaviour of the wave is dominated by the scattering phenomena. We introduce a scattering coefficient from [4, p. 22]

$$\rho = \frac{E_s}{E_r} \tag{9}$$

Here, E_r is the field specularly reflected (Θ_i=Θ_r) by a smooth and perfect conducting surface of similar dimensions as the rough one, and under the same angle of incidence at the same distance by considering horizontal polarization. From [4, Appendix A], we have

$$E_r = \frac{jkA\cos(\Theta_i)e^{jkd_0}}{\pi d_0} \tag{10}$$

The area A = $l_x\, l_y$ is the rectangular surface area and d_0 is the distance from the point of observation O to a reflection point on the rough surface. Importantly, the Kirchhoff solution requires the lateral dimension l_x and l_y of the area A to be much greater than the wavelength, i.e., $l_x \gg \lambda$ and $l_y \gg \lambda$.

The rough surfaces can be characterized by two statistical parameters: (i) the standard deviation height σ_h; (ii) the correlation length l_{corr}. The empirical parameters of the materials used in our modeling approach along with their standard deviation height and correlation length are tabulated in Table I. From a complex quantity ρ in (9), we determine the mean value of $|\rho|^2$

$$\langle \rho\rho^* \rangle = \left\langle |\rho|^2 \right\rangle = \left\langle \left| \frac{E_s^2}{E_r^2} \right| \right\rangle \tag{11}$$

Here, the operator $\langle . \rangle$ is an ensemble mean which represents a statistical average, and $(.)^*$ denotes the complex conjugate.

Now, assume a rectangular surface of area A = $l_x l_y$ with infinite conductivity. In general, the average scattering coefficient of an incident wave on a rough surface of angle Θ_i, scattered at angles Θ_r and Θ_s, respectively, is determined by the following expressions [4, p. 88]

$$\langle \rho\rho^* \rangle_\infty = \left(\rho_0^2 + \frac{\pi l_{corr}^2 F^2}{A} \sum_{m=1}^{\infty} \frac{g^m}{m!m} e^{-\frac{v_{xy}^2 l_{corr}^2}{4m}} \right) e^{-g} \tag{12}$$

The details about the expressions ρ_0, v_x, v_y, v_{xy}, F and g are given at [4, p. 88]. From expression in (12), it is apparent that the average scattering coefficient consists of two terms. The first term $\rho_0^2 e^{-g}$ describes the influence of the scattering in the direction of specular reflection (i.e., specular spike component) only, and the succeeding second term corresponds to the diffusely scattered field (i.e., side lobes components). The average scattering coefficient with different surface height distributions is schematically depicted in Fig. 3.

In the expression (12) it was assumed surface to be a perfect conductor. In this regard to approximate the average scattering coefficient for finite conductors, we average the conventional Fresnel reflection coefficient (Γ) over the entire surface area and use the resultant value ($\langle\Gamma\rangle$) as a constant in the Helmholtz integral [17]. To obtain the mean field and mean power scattered by finite conducting surfaces, we determine average scattering coefficient as [4, p. 98]

$$\langle \rho\rho^* \rangle_{\text{finite}} = \langle \Gamma\Gamma^* \rangle \langle \rho\rho^* \rangle_\infty \tag{13}$$

Therefore, the mean scattered power is given by

$$\langle P_s \rangle = \frac{\left|E_s^2\right|}{2Z_0} = \frac{\left|E_r^2\right|}{2Z_0} \langle \rho\rho^* \rangle_{\text{finite}} \tag{14}$$

Likewise, the incident power is

$$\langle P_i \rangle = \frac{\left|E_{\text{TX}}^2\right|}{2Z_0} \tag{15}$$

Thus, the average power reflection coefficient of a surface area A, specifying the scattered field in a distance r' from surface to the observation point O relative to the incident power P_i leading to [4, p. 89] and let $\left|E_{\text{TX}}^2\right| = 1$

$$\left\langle R_{power} \right\rangle_{sca} = \frac{\langle P_s \rangle}{\langle P_i \rangle} = \langle |E_r^2| \rangle \langle \rho\rho^* \rangle_{\text{finite}} \tag{16}$$

The significance of this result can be seen once we substitute the value of E_r from (10), we find

$$\left\langle R_{power} \right\rangle_{sca} = \frac{4A^2 \cos^2(\Theta_i)}{\lambda^2 r'^2} \langle \rho\rho^* \rangle_{\text{finite}} \tag{17}$$

The scattered field at the receiving point O has the following expression:

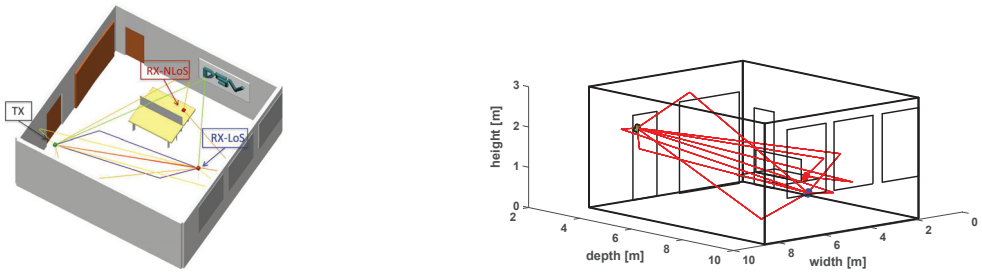

(a) (b)

Fig. 4: 3D layout of simulated real environment of the office room (a) Commercial ray-tracer and (b) Our self-programmed ray-tracing algorithm (wireframe).

TABLE I: MATERIALS PARAMETER (From [5, 10, 18]).

Material	$\tilde{\epsilon}_r$	$\tilde{\epsilon}_r$	l_{corr}	σ_h
Plaster X_i	3.691	0.217	1.70 mm	0.05 - 0.25 mm
PVC (ideally smooth)	2.788	0.069	-	0.00 mm
Wood (ideally smooth)	1.734	0.073	-	0.00 mm
Glass (ideally smooth)	6.656	0.539	-	0.00 mm

$$E_{\text{Scatt}}(O) = \left[G^{\text{RX}}_{\text{Scatt}}\right]^{*} \cdot \mathbf{H} \cdot G^{\text{TX}}_{\text{Scatt}} \cdot L_{\text{Scatt}} \cdot E_{\text{TX}} \qquad (18)$$

For B-K model, $\widetilde{\Gamma}_{\text{TE/TM}} = \sqrt{\langle R_{power,\,\text{TE/TM}} \rangle_{sca}}$. Notably, for diffuse scattering now from rough surfaces the terms ζ_1 and ζ_2 in $\mathbf{H}$ are not equal to zero. Rather, it is determined by the perturbation theory [15].

III. 3D RAY-TRACING ALGORITHM IMPLEMENTATION

The available commercial ray-tracer tools are incapable of considering the diffuse scattering (non-specular) due to surface roughness and can not be used without modifications [3], [16]. The commercial ray-tracer can barely determine the specular reflected paths with scattering losses due to surface roughness introduced. However, the diffuse scattering from non-specular directions will also impair the THz broadband channel behaviour [6] and must be included in the THz propagation modeling. In this section, we discuss the implementation of our novel and efficient ray-tracing algorithm based on B-K model. The RTA can be applied to different indoor scenarios such as offices, residential structures, conference rooms, corridors and libraries. It is noteworthy to mention that our self-programmed graphical user interface (GUI) based RTA works completely standalone. Moreover, our RTA can be integrated to any commercial ray-tracer tools.

A. Scenario

Simulations are conducted to evaluate the relative received power of a rough plaster with surface roughness $\sigma_h = 0.15$ mm including the angular and temporal information of the scattered multipaths with respect to the specular reflection directions. The office room of 3 m x 7 m x 7 m ascertains both line-of-sight and non-line-of-sight scenarios as shown in Fig. 4a. Up to twice-reflected paths have been considered in the modeling process. All walls and the ceiling are made with rough plasters given in Table I with focus to investigate and demonstrate the influence of degree of roughness on the 300 GHz propagation characteristics.

The transmitter is positioned in a corner of the office just below the ceiling at the point $x = 6$ m, $y = 1$ m, $z = 2$ m. The transmit output power was 0 dBm. Taking into account the table top terminals, both receivers are chosen to have the 0.75 m height at the point $x = 3.5$ m, $y = 4.45$ m, $z = 0.75$ m and $x = 1.7$ m, $y = 2.75$ m, $z = 0.75$ m, respectively. Moreover, the simulations were performed with omnidirectional antennas at both TX and RXs with radiation pattern in the azimuth plane to realize an estimation of the maximum occurring multipath influence, despite the demand of the terahertz frequencies for directional antennas of high gains. To maximize scattering contributions and lower scattering losses, vertically polarized antennas are chosen at both TX and RXs. Both RXs are 5 m apart from the TX. The single workplace have a height of 0.7 m, width of 1.8 m and length of 0.8 m. This workplace is separated by metallic panel of 1.8 m x 0.55 m dimensions and pine wooden tables with metallic legs. The three glass windows 1.65 x 1.7 m^2 each are modeled. These windows are 1.05 m above the floor and separated by a distance of 0.45 m from each other. The pine wood wardrobe of dimensions 2.25 x 2.6 x 0.1 m^3 is clearly depicted in Fig. 4a. The wooden door towards the corridor is 2.1 m high and 1.05 m wide. The other comparatively smaller door is 1.9 m high and 0.8 m wide.

B. Ray-Tracing Algorithm

Because rough surface area gives rise to many scattered paths around the specular reflection point, we have therefore considered N x N tiles around each specular point. Instead of considering the entire surface area as a single tile, we divide the surface into smaller square tiles like shown in Fig. 5.

In addition, the complex amplitude of the paths scattered from each tile is calculated according to the B-K model. Apart from the amplitude, the other propagation characteristics such as path length, polarization characteristics, propagation delay (ToA), and angular spreads (AoD, AoA) are associated with each path.
The significant steps of identifying clusters in the simulation process are as follows:

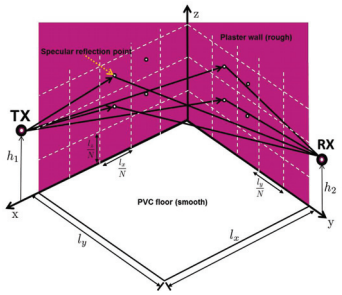

Fig. 5: Square tiling of the rough surface.

1) determine the specular reflection points either with a ray-tracing algorithm or by simulating the scattered environments using commercial ray-tracer (minimum path amplitude -150 dB).
2) layout 20 x 20 square tiles around each specular point with scattering area is equal to M times correlation length. From [6] 10 times gives a considerable difference power between specular and scattered paths around -220 dB.
3) take account of all angles (incidence, reflection, and scattering angle) for each path.
4) track all multipaths arriving at RX and calculate AoAs and AoDs to determine angular spread (minimum path amplitude -220 dB).
5) compute the individual powers of all the scattered multipaths from the tiles by applying the Kirchhoff equation (12).
6) calculate the received power by summing up the contributions of all the paths scattered from the tiles by applying Kirchhoff equation and polarization model (12).

IV. RESULTS AND ANALYSIS

To evaluate the functionality of the proposed ray-tracing algorithm, only specular reflections and non-specular diffuse scattered paths are considered in the simulation. The diffuse scattered paths are assumed to be coherent based on B-K model. To include polarization impact in the channel model, polarization characteristics of antennas and polarization characteristics of the propagation channel are also introduced. Note that the geometrical depolarization is treated utilizing the Jones calculus [12].

The results in Fig. 6 show the impact of surface roughness on the THz propagation channel and its influence on the received power in the specular direction. AoAs for LoS and N-LoS scenario have identical received power distribution for all the multipath. The non-specular multipaths around the specular reflection path emerges when the incident path hit the rough surface. However, only dominant paths around the specular reflection are considered in the simulation process (i.e., in our case maximum of 400 non-specular diffuse scattered paths). The RTA simulate this phenomenon accurately and agree well with literature which is affirmed in the previous section. We have used the threshold function of the RTA and set the receiver sensitivity to -220 dBm. However, below this limit, there is a little contribution from the diffuse scattered paths to the total received power. Moreover, AoDs power distribution shows fewer clusters than AoAs. Owing to the fact that for second-order reflections, RTA considers only specular paths from the first encountered surfaces by neglecting the diffuse scattered multipaths. This is due to the already reduced power of the scattered multipath after hitting the first surface. For LoS scenario, about 7944 specular and non-specular paths are considered. On the other hand, the RTA has found only 2568 valid multipaths for NLoS scenario.

Fig. 7 shows the clustered behaviour of time of arrival (ToA) distribution for azimuth plane with respect to AoA. The multipaths arrive with particular ToAs based on the different path lengths they cover. From the standpoint of geometrical analysis, the specular reflection should arrive earlier and consequently take up shorter ToA relative to scattered paths with longer ToAs (due to larger paths). Our simulation results revealed that such relation of ToA and AoA does not hold for all clusters due to their dependency on the complex propagation environment. Hence, our RTA' results conform with published in the literature.

V. CONCLUSIONS

A three-dimensional deterministic ray-tracing algorithm based on Beckmann-Kirchhoff model was developed and presented in this paper. This RTA is capable of simulating time-invariant multipath scattering model for the various indoor environments at terahertz frequencies. On top of that, common building materials with different surface roughness and correlation length covering line-of-sight as well as non-line-of-sight scenarios can be accurately simulated. The simulation results are validated by measurements from the literature of an earlier publication by modeling the similar LoS and NLoS scenarios for correctness and comparison. Moreover, the RTA provides output parameters for channel model simulation such as Received Power, Scattered Power, ToA, AoA, and AoD. Further, it needs to be extended to observe a scenario for the time-variant channels, where it also considers not only fixed but also moving objects.

ACKNOWLEDGEMENT

The research work presented in this paper has been funded by the German Research Foundation (Deutsche Forschungsgemeinschaft - DFG) under the framework of SFB TRR-196 for the Project M01.

REFERENCES

[1] V. Degli Esposti, "A Diffuse Scattering Model for Urban Propagation Prediction," *IEEE Transactions on Antennas and Propagation,*, vol. 49, no. 7, pp. 1111–1113, Jul. 2001.

[2] D. Didascalou et al., "An Approach to Include Stochastic Rough Surface Scattering Into Deterministic Ray-Optical Wave Propagation Modeling," *IEEE Transactions on Antennas and Propagation,*, vol. 51, no. 7, pp. 1508–1515, Jul. 2003.

[3] V. Degli Esposti et al., "An Advanced Field Prediction Model Including Diffuse Scattering," *IEEE Transactions on Antennas and Propagation,*, vol. 52, no. 7, pp. 1717–1728, Jul. 2004.

[4] P. Beckmann and A. Spizzichino, "The Scattering of Electromagnetic Waves from Rough Surfaces," *Artech House Radar Library*, USA, 1963.

[5] R. Piesiewicz et al., "Scattering Analysis for the Modeling of THz Communication Systems," in *IEEE Transactions on Antennas and Propagation*, vol. 55, no. 11, pp. 3002–3009, Nov. 2007.

[6] S. Priebe et al., "Non-specular Scattering Modeling for THz Propagation Simulations," *Proceedings of the 5th European Conference on Antennas and Propagation (EUCAP)*, pp. 1–5, May 2011.

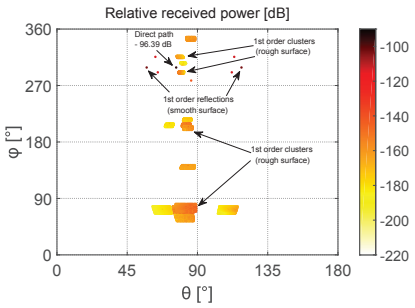

(a) AoA distribution of RX-LoS

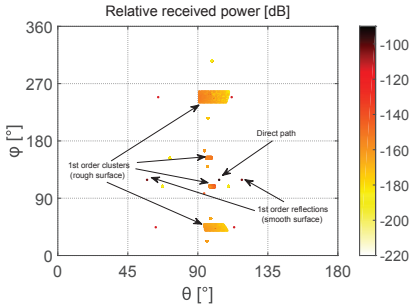

(b) AoD distribution of RX-LoS

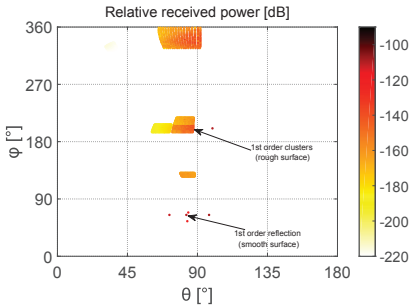

(c) AoA distribution of RX-NLoS

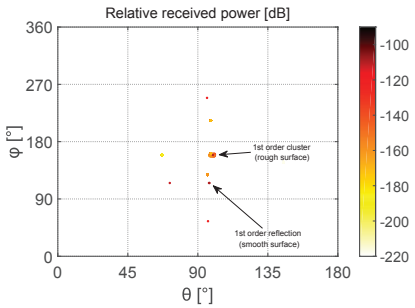

(d) AoD distribution of RX-NLoS

Fig. 6: Relative received power of AoA/AoDs in the azimuth and elevation plane of the office room. The frequency is 300 GHz, l_{corr} = 1.7 mm, $l_x = l_y$= 10 l_{corr}, and σ_h = 0.15 mm.

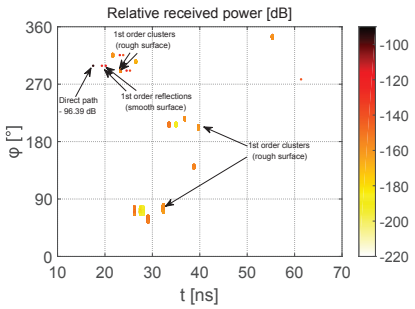

(a) ToA distribution of RX-LoS

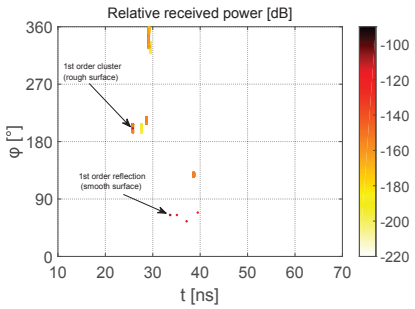

(b) ToA distribution of RX-NLoS

Fig. 7: Relative received power over ToA and AoA in the azimuth plane corresponding to Fig. 6.

[7] S. Priebe et al., "Channel and Propagation Measurements at 300 GHz," in *IEEE Transactions on Antennas and Propagation,*, vol. 59, no. 5, pp. 1688–1698, May 2011.

[8] C. Han, A. O. Bicen and I. F. Akyildiz, "Multi-Ray Channel Modeling and Wideband Characterization for Wireless Communications in the Terahertz Band," in *IEEE Transactions on Wireless Communications*, vol. 14, no. 5, pp. 2402–2412, May 2015.

[9] C. Oestges, B. Clerckx, L. Raynaud, and D. V. Janvier, "Deterministic Channel Modelling and Performance Simulation of Microcellular Wide-Band Communication Systems," in *IEEE Transactions on Vehicular Technology*, vol. 51, no. 6, Nov. 2002.

[10] R. Piesiewicz et al., "Terahertz Characterisation of Building Materials," in *Electronics Letters*, vol. 41, no. 18, pp. 1002–1004, Sep. 2005.

[11] A. Maltsev, R. Maslennikov, A. Lomayev, A. Sevastyanov, and A. Khoryaev, "IEEE 802.11-09/0431r0," Apr. 2009.

[12] A. Maltsev et al., "Channel Models for 60 GHz WLAN Systems," *IEEE 802.11-09/0334r8*, May 2010.

[13] M. Jacob et al., "Diffraction in mm and Sub-mm Wave Indoor Propagation Channels," *IEEE Transactions on Microwave Theory and Technique*, vol. 60, no.3, Mar. 2012.

[14] R. Kouyoumjian and P. Pathak, "Uniform Geometrical Theory of Diffraction for an Edge in a Perfectly Conducting Surface," *Proc. IEEE*, vol. 62, no.11, pp. 1448-1461, 1974.

[15] R. Vaughan and J. Andersen, "Channels, Propagation and Antennas for Mobile Communications." *IET*, 2003.

[16] C. Jansen et al., "Diffuse Scattering From Rough Surfaces in THz Communicaion Channels," *IEEE Transactions on Terahertz Science and Technology*, vol. 1, no.2, pp. 462–472, Nov. 2011.

[17] S. Nayar, K. Ikeuchi, and T. Kanade, "Surface reflection: physical and geometrical perspectives," *IEEE Transactions on Pattern Analysis and Machine Intelligence*, vol. 13, no. 7, pp. 611–634, 1991.

[18] R. Piesiewicz et al., "Properties of Building and Plastic Materials in the THz Range," *International Journal of Infrared and Millimeter Waves*, vol. 28, no. 5, pp. 363–371, May 2007.